Available online at www.sciencedirect.com

ScienceDirect

Nuclear Physics B 917 (2017) 317–336

NUCLEAR PHYSICS B

www.elsevier.com/locate/nuclphysb

Gauged $U(1)_{L_\mu - L_\tau}$ model in light of muon $g-2$ anomaly, neutrino mass and dark matter phenomenology

Sudhanwa Patra [a,*], Soumya Rao [b], Nirakar Sahoo [c], Narendra Sahu [c]

[a] *Center of Excellence in Theoretical and Mathematical Sciences, Siksha 'O' Anusandhan University, Bhubaeswar 751030, Odisha, India*

[b] *ARC Centre of Excellence for Particle Physics at the Terascale, Department of Physics, University of Adelaide, Adelaide, SA 5005, Australia*

[c] *Department of Physics, Indian Institute of Technology Hyderabad, Kandi, Sangareddy, Medak 502285, Telengana, India*

Received 29 November 2016; received in revised form 27 January 2017; accepted 18 February 2017
Available online 28 February 2017
Editor: Hong-Jian He

Abstract

Gauged $U(1)_{L_\mu - L_\tau}$ model has been advocated for a long time in light of muon $g-2$ anomaly, which is a more than 3σ discrepancy between the experimental measurement and the standard model prediction. We augment this model with three right-handed neutrinos (N_e, N_μ, N_τ) and a vector-like singlet fermion (χ) to explain simultaneously the non-zero neutrino masses and dark matter content of the Universe, while satisfying the anomalous muon $g-2$ constraints. We find that the model suffers stringent constraints from the simultaneous explanation of neutrino trident production and muon $g-2$ anomaly. In a large region of the parameter space, where contribution to muon $g-2$ anomaly comes partially and yet not ruled out by neutrino trident production, the model can explain the positron excess, observed at PAMELA, Fermi-LAT and AMS-02 through dark matter annihilation, while satisfying the relic density and direct detection limits.

* Corresponding author.
E-mail addresses: sudha.astro@gmail.com (S. Patra), soumya.rao@adelaide.edu.au (S. Rao), ph13p1005@iith.ac.in (N. Sahoo), nsahu@iith.ac.in (N. Sahu).

http://dx.doi.org/10.1016/j.nuclphysb.2017.02.010

1. Introduction

The standard model (SM) of elementary particle physics, which is based on the gauge group $SU(3)_C \times SU(2)_L \times U(1)_Y$, is very successful in explaining the fundamental interactions of nature. With the recent discovery of Higgs at LHC, the SM seems to be complete. However, it has certain limitations. For example, the muon $g-2$ anomaly, which is a discrepancy between the observation and SM prediction with more than 3σ confidence level [1]. Similarly, it does not explain sub-eV masses of active neutrinos as confirmed by long baseline oscillation experiments [2]. Moreover, it does not accommodate any particle candidate of dark matter (DM) whose existence is strongly supported by galaxy rotation curve, gravitational lensing and large scale structure of the universe [3]. In fact, the DM constitutes about 26.8% of the total energy budget of the universe as precisely measured by the satellite experiments, such as WMAP [4] and PLANCK [5].

At present LHC is the main energy frontier and is trying to probe many aspects of physics beyond the SM. An attractive way of probing new physics is to search for a Z'-gauge boson which will indicate an existence of $U(1)$ symmetry. Within the SM, we have accidental global symmetries $U(1)_B$, where B is the baryon number, and $U(1)_L$, where $L = L_e + L_\mu + L_\tau$ is the total lepton number. Note that $U(1)_B$ and $U(1)_L$ are anomalous and cannot be gauged without adding any ad hoc fermions to the SM. However, the differences between any two lepton flavors, i.e., $L_i - L_j$, with $i, j = e, \mu, \tau$, are anomaly free and can be gauged without any addition of extra fermions to the SM [6]. Among these extensions, the most discussed one is the gauged $L_\mu - L_\tau$ [7–40]. The interactions of the corresponding gauge boson Z' are restricted to only μ and τ families of leptons and therefore they significantly contribute to muon $g-2$ anomaly, which is a discrepancy between the observation and SM prediction with more than 3σ confidence level. Moreover, Z' does not have any coupling with the electron family. Therefore, it can easily avoid the LEP bound: $M'_Z/g' > 6$ TeV [41]. So, in this scenario a Z'-mass can vary from a few MeV to TeV which can in principle be probed at LHC and at future energy frontiers.

Gauged $U(1)_{L_\mu - L_\tau}$ models have been discussed extensively in the literature in light of sub-eV neutrino masses [19–34] and dark matter phenomenology [35–40]. All these models are devoted to predict either non-zero neutrino masses or dark matter content of the Universe, while satisfying the constraints from muon $g-2$ anomaly. We noticed that all the $U(1)_{L_\mu - L_\tau}$ models discussing dark matter phenomenology [35–40] predict a candidate of dark matter, which is elastic in nature.

In this paper we revisit the gauged $U(1)_{L_\mu - L_\tau}$ model in light of muon $g-2$ anomaly, non-zero neutrino mass and DM phenomenology simultaneously, while including the latest constraints from various observations. We found that the DM is required to be inelastic to reconcile the relic abundance constraints with null detection of DM at direct search experiments. We augment the SM by including three right handed neutrinos: N_e, N_μ and N_τ, which are singlets under the SM gauge group, and a vector like colorless neutral fermion χ. We also add an extra SM singlet scalar S. All these particles except N_e, are charged under $U(1)_{L_\mu - L_\tau}$, though singlets under the SM gauge group. When S acquires a vacuum expectation value (vev), the $U(1)_{L_\mu - L_\tau}$ breaks to identity and gives masses to Z' as well as to the neutral fermions N_e, N_μ, N_τ. We also impose an additional Z_2 symmetry under which χ is odd and all other fields are even. As a result χ serves as a candidate of DM. The smallness of neutrino mass is also explained using type-I see-saw with the presence of right handed neutrinos N_e, N_μ and N_τ, whose masses are generated from the vev of scalar field S.

In this model the relic abundance of DM (χ) is obtained via its annihilation to muon and tauon family of leptons through the exchange of $U(1)_{L_\mu - L_\tau}$ gauge boson Z'. We show that the

relic density crucially depends on $U(1)_{L_\mu - L_\tau}$ gauge boson mass $M_{Z'}$ and its coupling g'. In particular, we find that the observed relic density requires $g' \gtrsim 5 \times 10^{-3}$ for $M'_Z \gtrsim 100$ MeV. However, if $g' \lesssim 5 \times 10^{-3}$ then we get an over abundance of DM, while these couplings are compatible with the observed muon $g-2$ anomaly. We resolve this conflict by adding an extra singlet scalar η, doubly charged under $U(1)_{L_\mu - L_\tau}$, which can drain out the large DM abundance via the annihilation process: $\overline{\chi}\chi \to \eta^\dagger \eta$. As a result, the parameter space of the model satisfying muon $g-2$ anomaly can be reconciled with the observed relic abundance of DM. We also show that the acceptable region of parameter space for observed relic density and muon $g-2$ anomaly is further constrained by null detection of DM at Xenon-100 [42] and LUX [43]. Moreover, we noticed that the allowed parameter space is severely constrained by the neutrino trident production [44], the creation of a muon pair from the scattering of muon–neutrino off the coulomb field of a target nucleus. The neutrino trident production cross-section, reported by CHARM-II ($\sigma_{CHARM}/\sigma_{SM} = 1.58 \pm 0.57$) [45] and CCFR ($\sigma_{CCFR}/\sigma_{SM} = 0.82 \pm 0.28$) [46] collaborations, does not seem to deviate significantly from the SM prediction. On the other hand, a new Z' gauge boson, corresponding to a $U(1)_{L_\mu - L_\tau}$ gauge symmetry, contributes constructively to the production cross-section of the above mentioned process. In fact, combine constraints from muon $g-2$ anomaly and neutrino trident production restricts $M_{Z'} \lesssim 400$ MeV [44]. However, in a large region of the parameter space spanned by $M_{Z'} \gtrsim 400$ MeV and $g' \gtrsim 10^{-3}$, where contribution to muon $g-2$ anomaly comes partially and yet not ruled out by neutrino trident production, the positron excess, observed at PAMELA [47,48], Fermi-LAT [49] and AMS-02 [50,51], can be explained via the DM annihilation.

The paper is arranged as follows. In section 2, we describe in details the different aspects of the model. The constraint from big bang nucleosynthesis (BBN) [52–55] on the mixing angle of the new scalar field η with the Higgs field is discussed in section 3. Section 4 is devoted to show the allowed parameter space from muon $g-2$ anomaly. In section 5, we estimate the neutrino mass within the allowed parameter space. Sections 6, 7 and 8 are devoted to obtain constraints on model parameters from the relic density, direct and indirect search of DM. In section 9, we lay the conclusions with some outlook.

2. The model for muon $g-2$ anomaly, neutrino mass and dark matter

We consider the gauge extension of the SM with extra $U(1)_{L_\mu - L_\tau}$ symmetry (from now on referred to as "gauged $U(1)_{L_\mu - L_\tau}$ model") where difference between muon and tau lepton numbers is defined as a local gauge symmetry [6–40]. The advantage of considering the gauged $U(1)_{L_\mu - L_\tau}$ model is that the theory is free from any gauge anomaly without introduction of additional fermions. We break the gauge symmetry $U(1)_{L_\mu - L_\tau}$ and explore the possibility of having non-zero neutrino mass. An additional discrete Z_2 symmetry is also imposed under which χ is odd while all other fields are even. As a result χ emerges out as a candidate of DM.

2.1. Spontaneous symmetry breaking

The spontaneous symmetry breaking of gauged $U(1)_{L_\mu - L_\tau}$ model is given by

$$\mathcal{G}_{L_\mu - L_\tau} \xrightarrow{\langle S \rangle, \langle \eta \rangle} \mathcal{G}_{SM} \xrightarrow{\langle H \rangle} SU(3)_C \times U(1)_{\rm em}\,, \tag{1}$$

where

Table 1
Particle content of the minimal $U(1)_{L_\mu - L_\tau}$ gauge extension of the SM and their transformation under the SM gauge group.

	Field	$SU(3)_C \times SU(2)_L \times U(1)_Y$	L_μ	L_τ	$L_\mu - L_\tau$
Quarks	$Q_L \equiv (u,d)_L^T$	$(\mathbf{3},\mathbf{2},1/6)$	0	0	0
	u_R	$(\mathbf{3},\mathbf{1},2/3)$	0	0	0
	d_R	$(\mathbf{3},\mathbf{1},-1/3)$	0	0	0
Leptons	$L_e \equiv (\nu_e, e^-)_L^T$	$(\mathbf{1},\mathbf{2},-1/2)$	0	0	0
	$L_\mu \equiv (\nu_\mu, \mu^-)_L^T$	$(\mathbf{1},\mathbf{2},-1/2)$	1	0	1
	$L_\tau \equiv (\nu_\tau, \tau^-)_L^T$	$(\mathbf{1},\mathbf{2},-1/2)$	0	1	-1
	e_R	$(\mathbf{1},\mathbf{1},-1)$	0	0	0
	μ_R	$(\mathbf{1},\mathbf{1},-1)$	1	0	1
	τ_R	$(\mathbf{1},\mathbf{1},-1)$	0	1	-1
	N_e	$(\mathbf{1},\mathbf{1},0)$	0	0	0
	N_μ	$(\mathbf{1},\mathbf{1},0)$	1	0	1
	N_τ	$(\mathbf{1},\mathbf{1},0)$	0	1	-1
	χ	$(\mathbf{1},\mathbf{1},0)$	_	_	1
Scalars	H	$(\mathbf{1},\mathbf{2},1/2)$	_	_	0
	S	$(\mathbf{1},\mathbf{1},\ 0)$	_	_	1
	η	$(\mathbf{1},\mathbf{1},\ 0)$	_	_	2

$$\mathcal{G}_{L_\mu - L_\tau} \equiv SU(3)_C \times SU(2)_L \times U(1)_Y \times U(1)_{L_\mu - L_\tau}\,,$$
$$\mathcal{G}_{SM} \equiv SU(3)_C \times SU(2)_L \times U(1)_Y.$$

At first, the spontaneous symmetry breaking of $\mathcal{G}_{L_\mu - L_\tau} \to \mathcal{G}_{SM}$ is achieved by assigning non-zero vacuum expectation values (vevs) to complex scalar field S and η. The subsequent stage of symmetry breaking $\mathcal{G}_{SM} \to SU(3)_C \times U(1)_{\rm em}$ is obtained with the SM Higgs H providing masses to known charged fermions. The complete spectrum of the gauged $U(1)_{L_\mu - L_\tau}$ model in light of DM and neutrino mass is provided in Table 1 where the respective quantum numbers are presented under $SU(3)_C \times SU(2)_L \times U(1)_Y \times U(1)_{L_\mu - L_\tau}$. To the usual quarks and leptons, we have introduced additional neutral fermions N_e, N_μ, N_τ for light neutrino mass generation via seesaw mechanism and a vector like Dirac fermion χ for the candidate of DM, being odd under the imposed discrete symmetry Z_2.

2.2. Interaction Lagrangian

The complete interaction Lagrangian for the gauged $U(1)_{L_\mu - L_\tau}$ model is given by

$$\begin{aligned}
\mathcal{L}_{L_\mu - L_\tau} =\ & i\,\overline{N}_e \not{\partial} N_e + i\,\overline{N}_\mu \left(\not{\partial} + i\,g_{\mu\tau}\,Z'_\mu \gamma^\mu\right) N_\mu + i\,\overline{N}_\tau \left(\not{\partial} - i\,g_{\mu\tau}\,Z'_\mu \gamma^\mu\right) N_\tau \\
& - g_{\mu\tau}\left(\overline{\mu}\gamma^\mu \mu + \overline{\nu_\mu}\gamma^\mu P_L \nu_\mu - \overline{\tau}\gamma^\mu \tau - \overline{\nu_\tau}\gamma^\mu P_L \nu_\tau\right) Z'_\mu \\
& - M_{ee}\overline{N_e^c} N_e - (\lambda_{e\mu} S^\star \overline{N_e^c} N_\mu + \text{h.c.}) - (\lambda_{e\tau} S \overline{N_e^c} N_\tau + \text{h.c.}) \\
& - (\lambda_{\mu\mu}\eta^\star \overline{N_\mu^c} N_\mu + h.c) - (\lambda_{\tau\tau}\eta \overline{N_\tau^c} N_\tau + \text{h.c.}) \\
& - \left(Y_{ee}\overline{L_e}\tilde{H} N_e + Y_{\mu\mu}\overline{L_\mu}\tilde{H} N_\mu + Y_{\tau\tau}\overline{L_\tau}\tilde{H} N_\tau + \text{h.c.}\right) \\
& + i\,\overline{\chi}\left(\not{\partial} + i\,g_{\mu\tau}\,Z'_\mu \gamma^\mu\right)\chi - M_\chi \overline{\chi}\chi - f_\chi \overline{\chi^c}\chi\eta^\star \\
& - \frac{1}{4} F^{\mu\nu}_{Z'} F^{Z'}_{\mu\nu} + \frac{\epsilon}{4} F^{\mu\nu}_{Z'} F_{\mu\nu}
\end{aligned}$$

$$+|\left(\partial_\mu + i\, g_{\mu\tau}\, Z'_\mu\right) S|^2 - \mu_S^2 S^\dagger S + \lambda_S (S^\dagger S)^2 + |\left(\partial_\mu + i\, 2 g_{\mu\tau}\, Z'_\mu\right) \eta|^2$$
$$- \mu_\eta^2 \eta^\dagger \eta + \lambda_\eta (\eta^\dagger \eta)^2 + \lambda_{HS} (H^\dagger H)(S^\dagger S)$$
$$+ \lambda_{H\eta} (H^\dagger H)(\eta^\dagger \eta) + \lambda_{\eta S} (\eta^\dagger \eta)(S^\dagger S) + \mu_{\eta S} S S \eta^\star + \mathcal{L}_{\rm SM}\,. \tag{2}$$

Here $\mathcal{L}_{\rm SM}$ is the SM Lagrangian. We denote here Z'_μ as the new gauge boson for $U(1)_{L_\mu - L_\tau}$ and the corresponding field strength tensor as $F^{Z'}_{\mu\nu} = \partial_\mu Z'_\nu - \partial_\nu Z'_\mu$. The gauge coupling corresponding to $U(1)_{L_\mu - L_\tau}$ is defined as $g_{\mu\tau} \equiv g'$ (as mentioned in section 1).

2.3. Scalar masses and mixing

The scalar potential of the model is given by

$$\mathcal{V}(H, S) = -\mu_H^2 H^\dagger H + \lambda_H (H^\dagger H)^2 - \mu_\eta^2 \eta^\dagger \eta + \lambda_\eta (\eta^\dagger \eta)^2 - \mu_S^2 S^\dagger S + \lambda_S (S^\dagger S)^2$$
$$+ \lambda_{SH} (H^\dagger H)(S^\dagger S) + \lambda_{H\eta} (H^\dagger H)(\eta^\dagger \eta) + \lambda_{\eta S} (\eta^\dagger \eta)(S^\dagger S) + \mu_{\eta S} S S \eta^\star \tag{3}$$

where H is the SM Higgs doublet and S, η are the complex scalar singlets under SM, while charged under $U(1)_{L_\mu - L_\tau}$. The neutral complex scalars H^0, S and η can be parametrized as follows:

$$H^0 = \frac{1}{\sqrt{2}}(v_H + h) + \frac{i}{\sqrt{2}} G^0\,,$$
$$S = \frac{1}{\sqrt{2}}(v_S + s) + \frac{i}{\sqrt{2}} A\,,$$
$$\eta = \frac{1}{\sqrt{2}}(v_\eta + \eta) + \frac{i}{\sqrt{2}} B\,. \tag{4}$$

The mass matrix for the neutral scalars is given by

$$\mathcal{M}^2 = \begin{pmatrix} 2\lambda_H\, v_H^2 & \lambda_{SH}\, v_H\, v_S & \lambda_{H\eta}\, v_H\, v_\eta \\ \lambda_{SH}\, v_H\, v_S & 2\lambda_S\, v_S^2 & \lambda_{\eta S}\, v_S\, v_\eta + \mu_{\eta S}\, v_S \\ \lambda_{H\eta}\, v_H\, v_\eta & \lambda_{\eta S}\, v_S\, v_\eta + \mu_{\eta S}\, v_S & 2\lambda_\eta\, v_\eta^2 \end{pmatrix}. \tag{5}$$

This is a symmetric mass matrix. So it can be diagonalized by a unitary matrix:

$$V^\dagger \mathcal{M}^2 V = \text{Diagonal}(M_h^2,\, M_S^2,\, M_\eta^2). \tag{6}$$

We identify M_h as the physical mass of the SM Higgs, while M_S and M_η are the masses of additional scalars S and η respectively. Since S and η are singlets, their masses can vary from sub-GeV to TeV region. For a typical set of values: $v_H = 174$ GeV, $v_S = 1200$ GeV, $v_\eta = 50$ GeV, $\lambda_H = 0.2585$, $\lambda_{SH} = 0.0005$, $\lambda_S = 0.4$, $\lambda_\eta = 0.00021$, $\lambda_{\eta H} = 0.00001$, $\lambda_{\eta S} = 0.0015$, $\mu_{\eta S} = 0.1$ GeV, the physical masses are found to be $M_h = 125$ GeV, $M_S = 1073$ GeV, $M_\eta = 1$ GeV and the mixing between h and η field is $\sin\theta_{\eta h} = 5.56 \times 10^{-6}$. We will study the importance of η field while calculating the relic abundance of DM. The mixing between η and h field is required to be small as it plays a dominant role in the direct detection of DM. We will show in Fig. 5 that if the mixing angle is large then it will kill almost all the relic abundance parameter space.

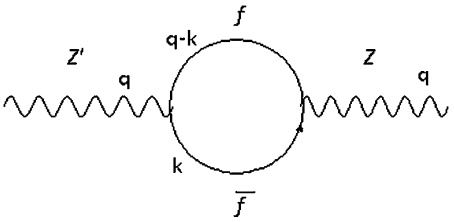

Fig. 1. The mixing between the SM gauge boson Z and the $U(1)_{L_\mu - L_\tau}$ gauge boson Z' arising through the exchange of muon and tauon families of leptons.

2.4. Mixing in the gauge sector

The breaking of gauged $U(1)_{L_\mu - L_\tau}$ symmetry by the vev of S and η gives rise to a massive neutral gauge boson Z' which couples to only muon and tauon families of leptons. In the tree level there is no mixing between the SM gauge boson Z and Z'. However at one loop level, there is a mixing between Z and Z' through the exchange of muon and tauon families of leptons as shown in the Fig. 1. The loop factor can be estimated as

$$\Pi^{\mu\nu}(q^2) = -\left(q^2 g^{\mu\nu} - q^\mu q^\nu\right)\frac{1}{3}\frac{1}{16\pi^2}\left(g_{\mu\tau}\frac{C_V g}{2\cos\theta_W}\right)\mathrm{Log}\left(\frac{m_f^2}{\Lambda^2}\right) \tag{7}$$

where θ_W is the Weinberg angle, C_V is the vector coupling of SM fermions with Z boson, Λ is the cut off scale of the theory and m_f is the mass of the charged fermion running in the loop. In the gauge basis, the mass matrix is given by

$$\mathcal{M}_2^2 = \begin{pmatrix} M_{Z_0}^2 & \Pi \\ \Pi & \tilde{M}_{Z'}^2 \end{pmatrix} \tag{8}$$

where Π is given by $\Pi = \Pi^{\mu\nu} * g_{\mu\nu}$ and $M_{Z_0} = 91.1876$ GeV. Thus the mixing angle is given by

$$\tan 2\theta_Z = \frac{2\Pi}{\tilde{M}_{Z'}^2 - M_{Z_0}^2}. \tag{9}$$

Diagonalizing the mass matrix (8) we get the eigen-values:

$$\begin{aligned} M_Z^2 &= \frac{M_{Z^0}^2 - M_{Z'}^2 \sin^2\theta_Z}{\cos^2\theta_Z}, \\ M_{Z'}^2 &= \frac{\tilde{M}_{Z'}^2 - M_Z^2 \sin^2\theta_Z}{\cos^2\theta_Z} \end{aligned} \tag{10}$$

where M_Z and $M_{Z'}$ are the physical masses of Z and Z' gauge bosons. The mixing angle θ_Z has to be chosen in such a way that the physical mass of Z-boson should be obtained within the current uncertainty of the SM Z boson mass [56]. It can be computed from equation (10) as follows:

$$\frac{M_Z - M_{Z^0}}{M_{Z^0}} = \frac{M_{Z^0}^2 - M_{Z'}^2}{2M_{Z^0}^2}\tan^2\theta_Z \leq 4.6 \times 10^{-5}. \tag{11}$$

For $M_{Z'} - M_{Z^0} \gtrsim M_{Z^0}$ we get $\tan\theta_Z \lesssim 10^{-2}$.

3. BBN constraint on η–h mixing

The scalar η does not decay to SM particles directly. However it can decay to SM fermions through η–h mixing. The decay width is given by

$$\Gamma_\eta \simeq \sum_{2m_f < M_\eta} \frac{M_\eta}{8\pi}\theta_{\eta h}^2 \frac{2m_f^2}{v_H^2}\,, \tag{12}$$

where m_f is the mass of the SM fermion. Thus lifetime of η is estimated to be

$$\tau_\eta \simeq 1s \times \left(\frac{\theta_{\eta h}}{10^{-6}}\right)^{-2} \left(\frac{1\ \text{GeV}}{M_\eta}\right). \tag{13}$$

For η to decay before big bang nucleosynthesis (BBN) we demand that $\tau_\eta \lesssim \tau_{BBN} \sim 1$ s [52–55], so that it does not affect the predictions of BBN. Therefore we get $\theta_{\eta h} \gtrsim \mathcal{O}(10^{-6})$ for $M_\eta \gtrsim 1$ GeV. We will see that the parameter space is well compatible with BBN constraint for direct detection as well as the relic abundance of DM in subsequent sections.

4. Muon $g-2$ anomaly

The magnetic moment of muon is given by

$$\overrightarrow{\mu_\mu} = g_\mu \left(\frac{q}{2m}\right)\overrightarrow{S}\,, \tag{14}$$

where g_μ is the gyromagnetic ratio and its value is 2 for a structureless, spin $\frac{1}{2}$ particle of mass m and charge q. Any radiative correction, which couples to the muon spin to the virtual fields, contributes to its magnetic moment and is given by

$$a_\mu = \frac{1}{2}(g_\mu - 2). \tag{15}$$

At present there is a more than 3σ discrepancy between the experimental measurement [57] and the SM prediction [1] of a_μ value. This is given by

$$\Delta a_\mu = a_\mu^{expt} - a_\mu^{SM} = (295 \pm 88) \times 10^{-11}\,. \tag{16}$$

In the present model, the new gauge boson Z' contributes to Δa_μ and is given by [40]

$$\Delta a_\mu = \frac{\alpha'}{2\pi}\int_0^1 dx \frac{2m_\mu^2 x^2(1-x)}{x^2 m_\mu^2 + (1-x)M_{Z'}^2} \approx \frac{\alpha'}{2\pi}\frac{2m_\mu^2}{3M_{Z'}^2}\,, \tag{17}$$

where $\alpha' = g_{\mu\tau}^2/4\pi$. The above equation implies that the discrepancy between the experimental measurement [57] and the SM prediction [1] of a_μ value can be explained in a large region of parameter space as shown by black shaded region in Fig. 3. Thus any value of $(g_{\mu\tau}, M_{Z'})$ below the black shaded region is insufficient to account for anomalous $g-2$ values, while the corresponding points above the black shaded region give excess $g-2$ values.

5. Neutrino mass

In order to account for tiny non-zero neutrino masses for light neutrinos, we extend the minimal gauged $U(1)_{L_\mu - L_\tau}$ model with additional neutral fermions $N_e(0), N_\mu(1), N_\tau(-1)$ where the quantum numbers in the parentheses are the $L_\mu - L_\tau$ charge. The relevant Yukawa interaction terms are given by

$$\begin{aligned}\mathcal{L} &= -\frac{1}{2}M_{ee}\overline{N_e^c}N_e - \frac{1}{2}M_{\mu\tau}\overline{N_\mu^c}N_\tau - (\lambda_{e\mu}S^\star\overline{N_e^c}N_\mu + \text{h.c.}) - (\lambda_{e\tau}S\overline{N_e^c}N_\tau + \text{h.c.}) \\ &\quad - (\lambda_{\mu\mu}\eta^\star\overline{N_\mu^c}N_\mu + \text{h.c.}) - (\lambda_{\tau\tau}\eta\overline{N_\tau^c}N_\tau + h.c) \\ &\quad - \left(Y_{ee}\overline{L_e}\tilde{H}N_e + Y_{\mu\mu}\overline{L_\mu}\tilde{H}N_\mu + Y_{\tau\tau}\overline{L_\tau}\tilde{H}N_\tau + \text{h.c.}\right) \\ &= \frac{1}{2}N_\alpha^T\mathcal{C}^{-1}M_{R\alpha\beta}N_\beta + M_{D\alpha\beta}\overline{\nu_\alpha}N_\beta + \text{h.c.} \end{aligned} \tag{18}$$

where the Dirac and Majorana neutrino mass matrices are given by

$$M_R = \begin{pmatrix} M_{ee} & \lambda_{e\mu}v_S & \lambda_{e\tau}v_S \\ \lambda_{e\mu}v_S & \lambda_{\mu\mu}v_\eta & M_{\mu\tau} \\ \lambda_{e\tau}v_S & M_{\mu\tau} & \lambda_{\tau\tau}v_\eta \end{pmatrix}, \quad M_D = \begin{pmatrix} Y_{ee}v_H & 0 & 0 \\ 0 & Y_{\mu\mu}v_H & 0 \\ 0 & 0 & Y_{\tau\tau}v_H \end{pmatrix}. \tag{19}$$

Using seesaw approximation, the light neutrino mass matrix can be read as

$$m_\nu \simeq -M_D M_R^{-1} M_D^T. \tag{20}$$

We illustrate here a specific scenario where not only the resulting Dirac neutrino mass matrix is diagonal but also degenerate. As a result, we can express $M_D = m_d \mathbb{I}_{3\times 3}$. One can express heavy Majorana neutrino mass matrix in terms of light neutrino mass matrix as

$$M_R = m_d^2 m_\nu^{-1}. \tag{21}$$

Thus, one can reconstruct M_R using neutrino oscillation parameters and $m_d \simeq 10^{-4}$ GeV. As we know that light neutrino mass matrix is diagonalized by the PMNS mixing matrix as

$$m_\nu^{\text{diag.}} = U_{\text{PMNS}}^\dagger m_\nu U_{\text{PMNS}}^* = \text{diag.}\{m_1, m_2, m_2\}$$

where m_i are the light neutrino mass eigenvalues. The PMNS mixing matrix is generally parameterized as

$$U_{\text{PMNS}} = \begin{pmatrix} c_{12}c_{13} & s_{12}c_{13} & s_{13}e^{-i\delta} \\ -s_{12}c_{23} - c_{12}s_{13}s_{23}e^{i\delta} & c_{12}c_{23} - s_{12}s_{13}s_{23}e^{i\delta} & c_{13}s_{23} \\ s_{12}s_{23} - c_{12}s_{13}c_{23}e^{i\delta} & -c_{12}s_{23} - s_{12}s_{13}c_{23}e^{i\delta} & c_{13}c_{23} \end{pmatrix} \cdot P \tag{22}$$

where $c_{ij} \equiv \cos\theta_{ij}$, $s_{ij} \equiv \sin\theta_{ij}$ (for $ij = 12, 13, 23$), and $P = \text{diag.}\{1, e^{i\alpha}, e^{i\beta}\}$. Here we denoted Dirac phase as δ and Majorana phases as α, β.

For a numerical example, we consider the best-fit values of the oscillation parameters, the atmospheric mixing angle $\theta_a \equiv \theta_{23} \simeq 41.2^\circ$, solar angle $\theta_s \equiv \theta_{12} \simeq 34.2^\circ$, the reactor mixing angle $\theta_r \equiv \theta_{13} \simeq 9^\circ$, and the Dirac CP phase $\delta = 0.8\pi$ (Majorana phases assumed to be zero here for simplicity i.e., $\alpha, \beta = 0$). The PMNS mixing matrix for this best-fit oscillation parameters is estimated to be

$$U_{\text{PMNS}} = \begin{pmatrix} 0.8168 & 0.5552 & -0.1265 - 0.0919\,i \\ -0.3461 - 0.0510\,i & 0.6604 - 0.0347\,i & 0.6634 \\ 0.4551 - 0.0563\,i & -0.5028 - 0.0382\,i & 0.7316 \end{pmatrix}. \tag{23}$$

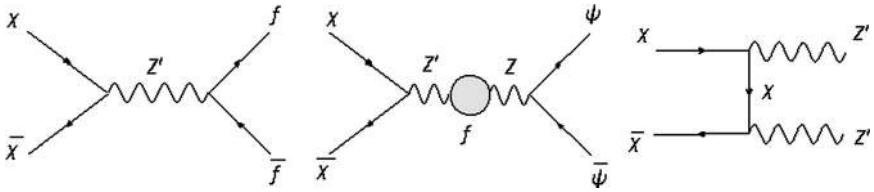

Fig. 2. Possible annihilation channels for relic abundance of DM, where f represents muon and tauon families of leptons while ψ represents the SM fermion.

We also use the best-fit values of mass squared differences $\Delta m^2_{\rm s} \equiv m^2_2 - m^2_1 = 2.5 \times 10^{-5}$ eV^2 and $\Delta m^2_{\rm a} \equiv |m^2_3 - m^2_1| = 7.56 \times 10^{-3}$ eV^2. As we do not know the sign of $\Delta m^2_{\rm a}$, the pattern of light neutrinos could be normal hierarchy (NH) with $m_1 < m_2 < m_3$,

$$m_2 = \sqrt{m^2_1 + \Delta m^2_{\rm s}}\,, \qquad m_3 = \sqrt{m^2_1 + \Delta m^2_{\rm a}}\,,$$

or, the inverted hierarchy (IH) with $m_3 < m_1 < m_2$,

$$m_1 = \sqrt{m^2_3 + \Delta m^2_{\rm a}}\,, \qquad m_2 = \sqrt{m^2_3 + \Delta m^2_{\rm a} + \Delta m^2_{\rm s}}\,.$$

Now, one can use these oscillation parameters and $m_d \simeq 10^{-4}$ GeV, the mass matrix for heavy neutrinos is expressed as

$$M_R = 10^{-8}\,{\rm GeV}^2 \left(U_{\rm PMNS} m_\nu^{\rm diag.} U^T_{\rm PMNS}\right)^{-1}\,. \tag{24}$$

Using $m_1 = 0.001$ eV, the masses for heavy neutrinos are found to be $M_{N_1} \simeq 100$ GeV, $M_{N_2} \simeq 1000$ GeV and $M_{N_3} \simeq 8000$ GeV. The same algebra can be extended for inverted hierarchy and quasi-degenerate pattern of light neutrinos for deriving structure of M_R.

6. Relic abundance of dark matter

Under the discrete symmetry Z_2, as mentioned in section 2, χ is odd and all other fields are even. As a result χ becomes a viable candidate for DM. We explore the parameter space allowed by relic abundance and null detection of DM at direct search experiments in the following two cases:

(A) in absence of η;
(B) in presence of η.

6.1. Relic abundance in absence of η

For simplicity, we assume that the right handed neutrinos N_μ and N_τ as well as the scalar field S are heavier than the χ mass. Now in absence of η,[1] the relevant diagrams that contribute to the relic abundance of χ are shown in Fig. 2. Since the null detection of DM at direct search experiments, such as Xenon-100 and LUX restricts the Z–Z' mixing to be small ($\tan\theta_z < 10^{-2}$), the dominant contribution to relic abundance, below the threshold of Z', comes from the s-channel

[1] In absence of η the neutrino mass will not be affected.

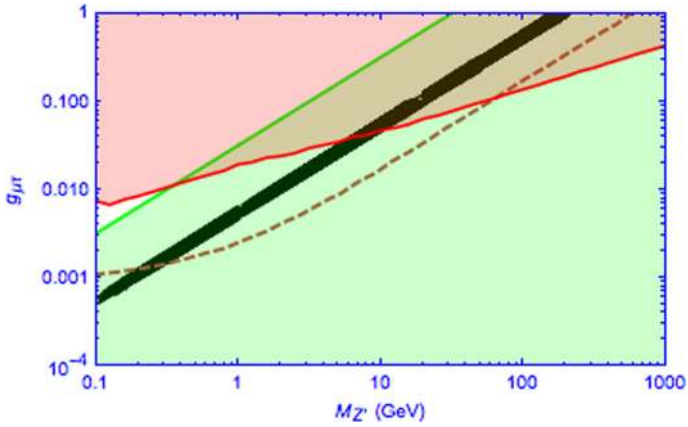

Fig. 3. Parameter space for Z' boson. The region above the red line is allowed by the correct relic abundance of DM, the green shaded region is allowed by null detection of DM at LUX using Z–Z' mixing to be 10^{-3}. Black shaded region is allowed by muon $g-2$ anomaly. Neutrino trident production [44] forbids the region above the dashed brown curve. (For interpretation of the references to color in this figure, the reader is referred to the web version of this article.)

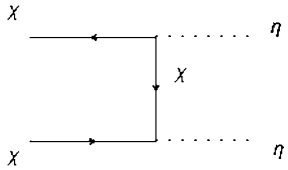

Fig. 4. Dominant annihilation channel for relic abundance of DM in the region of small $g_{\mu\tau}$.

annihilation: $\bar{\chi}\chi \to \bar{\psi}\psi$, $\bar{f}f$ through the exchange of Z'. Due to the resonance effect this cross-section dominates. We have shown in Fig. 3, the correct relic abundance of DM in the plane of $M_{Z'}$ and $g_{\mu\tau}$. Below the red line the annihilation cross-section through Z' exchange is small due to small gauge coupling and therefore, we always get an over abundance of DM. The constraints from muon $g-2$ anomaly, shown by black shaded region, and direct detection of DM via Z–Z' mixing, shown by green shaded region using Z–Z' mixing to be 10^{-3}, are given in the same plot for comparison purpose. We note that region above green line is allowed by direct detection if Z–Z' mixing is less than 10^{-3}. We have also shown the constraint from the neutrino trident production [44] by the brown dashed curve. The region above the brown dashed curve is ruled out due to the mismatch between experimental observation [45,46] and SM prediction induced by large gauge coupling ($g_{\mu\tau}$). This implies that the combine constraints from muon $g-2$ anomaly and neutrino trident production rules out Z' mass more than 400 MeV and $g_{\mu\tau} \gtrsim 10^{-3}$. On the other hand, for $M_{Z'} \lesssim 400$ MeV and $g_{\mu\tau} \lesssim 10^{-3}$ we get an overabundance of DM. We resolve this issue by adding an extra singlet scalar field $\eta(2)$, where the number inside the parenthesis is the charge under $U(1)_{L_\mu - L_\tau}$.

6.2. *Relic abundance in presence of η*

In presence of the SM singlet scalar field $\eta(2)$, the new annihilation channels $\bar{\chi}\chi \to \eta^\dagger\eta$, shown in Fig. 4, and $\bar{\chi}\chi \to h\eta$ open up in addition to the earlier mentioned channels, shown in Fig. 2. However, in the region of small gauge coupling $g_{\mu\tau}$, the dominant channel for the relic

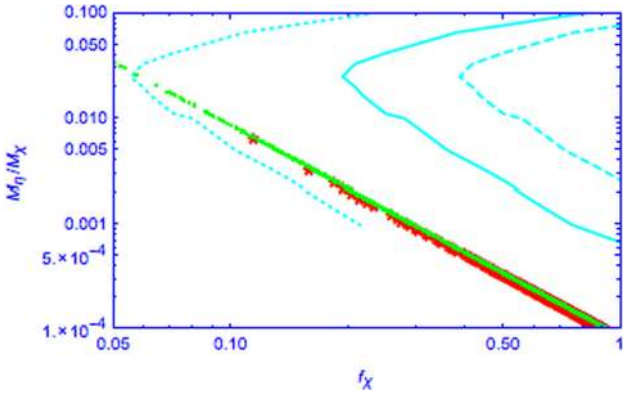

Fig. 5. Constraints on the parameter space satisfying correct relic abundance (shown by green and red points) and null detection of dark matter at LUX (shown by cyan lines). For $M_\eta = 1$ GeV, we have used $\sin\theta_{\eta h} = 5 \times 10^{-6}$ (dashed-line), 1×10^{-5} (solid-line) and 3.5×10^{-5} (dotted-line). (For interpretation of the references to color in this figure, the reader is referred to the web version of this article.)

abundance of DM is $\bar{\chi}\chi \to \eta^\dagger\eta$. The other channel: $\bar{\chi}\chi \to h\eta$ is suppressed due to the small mixing angle $\sin\theta_{\eta h}$, required by null detection of DM at direct search experiments. We assume that the mass of η to be order of a GeV as discussed in section 2.3. In this case the analytic expression for the cross-section of $\bar{\chi}\chi \to \eta^\dagger\eta$ is given by

$$\langle\sigma|v|\rangle(\chi\chi \to \eta\eta) = \frac{1}{128\pi}\frac{1}{\left(1-\frac{M_\eta^2}{2M_\chi^2}\right)^2}\frac{f_\chi^4}{M_\chi^2}\left(1-\frac{M_\eta^2}{M_\chi^2}\right)^{3/2}. \tag{25}$$

From the above expression we observe that the cross-section goes as $\frac{f_\chi^4}{M_\chi^2}$ for $M_\eta \ll M_\chi$. Fixing $M_\eta = 1$ GeV and varying the DM mass M_χ and the coupling f_χ, we have shown in Fig. 5 the allowed region in the plane of M_η/M_χ and f_χ for the correct relic abundance. The green points show the value of analytic approximation (25), while the red points reveal the result from full calculation using `micrOMEGAs` [58]. The matching of both points indicates that the contribution to relic abundance is solely coming from the $\bar{\chi}\chi \to \eta^\dagger\eta$ channel. From Fig. 5 it is clear that as the ratio $\frac{M_\eta}{M_\chi}$ decreases, i.e., M_χ increases for a fixed value of M_η, we need a large coupling to get the correct relic abundance. For comparison, we also show the DM-nucleon spin independent elastic cross-section: $\chi n \to \chi n$ mediated through the η–h mixing, in the same plot. We find that the allowed mixing angle by LUX data is quite small. Typically, for $M_\eta \gtrsim 1$ GeV, we need $\theta_{\eta h} \lesssim \mathcal{O}(10^{-5})$ to reconcile the relic abundance with LUX data.

7. Direct detection

We constrain the model parameters from null detection of DM at direct search experiments such as Xenon-100 [42] and LUX [43] in the following two cases:

a. In the absence of η;
b. In the presence of η.

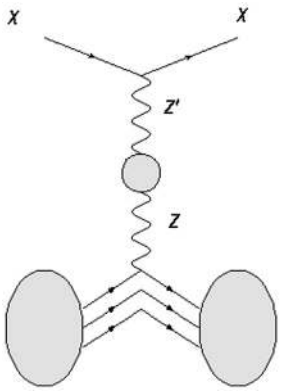

Fig. 6. Feynman diagrams for direct detection of DM through scattering with nuclei via the exchange of Z–Z' mixing.

We show that in absence of η field, the elastic scattering of DM with nucleon through Z–Z' mixing give stringent constraint on the model parameters: $M_{Z'}$ and $g_{\mu\tau}$, as depicted in Fig. 3. On the other hand, in the presence of η field, the elastic scattering will be possible through the η–h mixing, while inelastic scattering with nucleon will be possible via Z–Z' mixing. In the following we discuss in details the possible constraints on model parameters.

7.1. Direct detection in absence of η

While the direct detection of DM through its elastic scattering with nuclei is a very challenging task, the splendid current sensitivity of present direct DM detection experiments might allow to set stringent limits on parameters of the model, or hopefully enable the observation of signals in near future. In absence of η field, the elastic scattering between singlet fermion DM with nuclei is displayed in Fig. 6.

The spin independent DM-nucleon cross-section mediated via the loop induced Z–Z' mixing is given by [59,60]

$$\sigma_{\rm SI}^{Z} = \frac{1}{64\pi A^2}\mu_r^2 \tan^2\theta_Z \frac{G_F}{2\sqrt{2}}\frac{g_{\mu\tau}^2}{M_{Z'}^2}\left[Z\frac{f_p}{f_n} + (A-Z)\right]^2 f_n^2\,, \tag{26}$$

where A is the mass number of the target nucleus, $\mu_r = M_\chi m_n/(M_\chi + m_n) \approx m_n$ is the reduced mass, m_n is the mass of nucleon (proton or neutron) and f_p and f_n are the interaction strengths (including hadronic uncertainties) of DM with proton and neutron respectively. Here Z is the atomic number of the target nucleus.

For simplicity we assume conservation of isospin, i.e. $f_p/f_n = 1$. The value of f_n is varied within the range: $0.14 < f_n < 0.66$ [61]. If we take $f_n \simeq 1/3$, the central value, then from Eq. (26) we get the total cross-section per nucleon to be

$$\sigma_{\rm SI}^{Z} \simeq 7.6\times 10^{-46}\ {\rm cm}^2 \tan^2\theta_Z \frac{g_{\mu\tau}^2}{M_{Z'}^2} \tag{27}$$

for the DM mass of 33 GeV.

The Z-boson mass puts a stringent constraint on the mixing parameter $\tan\theta_Z$ to be $\tan\theta_Z < 10^{-2}$ [62,63]. For $\tan\theta_Z = 10^{-3}$ we show the allowed values of $g_{\mu\tau}$ and $M_{Z'}$ in Fig. 3 by choosing LUX limit on spin independent direct DM detection cross-section to be 7.6×10^{-46} cm^2

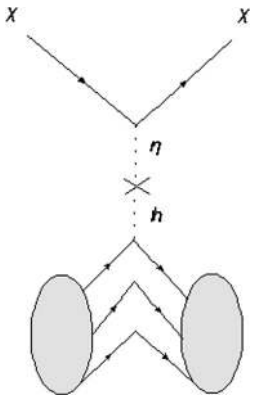

Fig. 7. Elastic scattering of DM with nuclei through η–h mixing.

(at a DM mass of 33 GeV). The plot follows a straight line as expected from equation (26) and shown by the green line in Fig. 3. Any values below that line will be allowed by the LUX limit. However the space above the green line will also be allowed if we choose $\tan\theta_Z < 10^{-3}$. In other words, the parameters $g_{\mu\tau}$ and $M_{Z'}$ are not severely constrained by the direct detection of DM.

7.2. Direct detection in presence of η

In presence of the η field both elastic and inelastic scattering between DM and the nuclei is possible. The elastic scattering is mediated through η–h mixing while inelastic scattering is mediated by the Z–Z' mixing.

7.2.1. Elastic scattering of dark matter

The spin-independent scattering of DM with nuclei is a t-channel exchange diagram as shown in Fig. 7 through the mixing of scalar singlet η with the SM Higgs H. The elastic scattering cross section σ^n_{SI} off a nucleon is given by [59,60]

$$\sigma^{\eta h}_{\rm SI} = \frac{\mu_r^2}{\pi A^2}\left[Z f_p + (A-Z) f_n\right]^2 \tag{28}$$

where μ_r is the reduced mass, Z and A are respectively atomic and mass number of the target nucleus. In the above equation f_p and f_n are the effective interaction strengths of the DM with the proton and neutron of the target nucleus and are given by

$$f_{p,n} = \sum_{q=u,d,s} f^{p,n}_{T_q}\alpha_q \frac{m_{p,n}}{m_q} + \frac{2}{27} f^{p,n}_{TG} \sum_{q=c,t,b} \alpha_q \frac{m_{p,n}}{m_q} \tag{29}$$

with

$$\alpha_q = \frac{f_\chi \sin\theta_{\eta h}}{M_\eta^2}\left(\frac{m_q}{v_H}\right). \tag{30}$$

In Eq. (29), the different coupling strengths between the DM and light quarks are given by [3,64,65] $f^{(p)}_{Tu} = 0.020 \pm 0.004$, $f^{(p)}_{Td} = 0.026 \pm 0.005$, $f^{(p)}_{Ts} = 0.118 \pm 0.062$, $f^{(n)}_{Tu} = 0.014 \pm 0.004$, $f^{(n)}_{Td} = 0.036 \pm 0.008$, $f^{(n)}_{Ts} = 0.118 \pm 0.062$. The coupling of DM with the gluons in target nuclei is parameterized by

$$f^n_{TG} = 1 - \sum_{q=u,d,s} f^n_{Tq}\,. \tag{31}$$

Thus from Eqs. (28), (29), (30), (31), the spin-independent DM-nucleon interaction through η–h mixing is given by

$$\sigma^{\eta h}_{SI} = \frac{\mu_r^2 f_\chi^2 \sin^2\theta_{\eta h}}{\pi A^2 M_\eta^4}\Bigg[Z\frac{m_p}{v_H}\left(f^p_{T_u} + f^p_{T_d} + f^p_{T_s} + \frac{2}{9}f^p_{TG}\right) + (A-Z)\frac{m_n}{v_H}\left(f^n_{T_u} + f^n_{T_d} + f^n_{T_s} + \frac{2}{9}f^n_{TG}\right)\Bigg]^2. \tag{32}$$

In the above equation, the unknowns are f_χ, $\sin\theta_{\eta h}$ and M_η. So using the current limit on spin-independent scattering cross-section from Xenon-100 [42] and LUX [43] one can constrain these parameters f_χ and M_η for a fixed value of mixing angle $\sin\theta_{\eta h}$. Here we use LUX bound and the corresponding contour lines are drawn in the Fig. 5 by choosing $M_\eta = 1$ GeV (cyan lines). We have drawn three contour lines for three different values of mixing angles: $\sin\theta_{\eta h} = 5\times10^{-6}$ (dashed), $\sin\theta_{\eta h} = 10^{-5}$ (solid) and $\sin\theta_{\eta h} = 3.5\times10^{-5}$ (dotted). The regions on the right of the respective lines are excluded by LUX data. From Fig. 5, we see that for a constant value of M_η, if $\sin\theta_{\eta h}$ decreases then the curves shift towards higher value of f_χ. Thus for a typical value of η mass: $M_\eta = 1$ GeV, we need $\theta_{\eta h} \lesssim \mathcal{O}(10^{-5})$ to be compatible with relic abundance as well as direct search of DM at LUX. This constraint is also in agreement with bound from BBN as discussed in section 3.

7.2.2. Inelastic scattering of dark matter

As we discussed above inelastic scattering [66] of the DM with the target nuclei is also possible via Z–Z' mixing. Let us rewrite the DM Lagrangian in presence of η field as [67–70]

$$\mathcal{L}_{DM} = i\,\overline{\chi}\left(\not{\partial} + i\,g_{\mu\tau}\,Z'_\mu\gamma^\mu\right)\chi - M_\chi\,\overline{\chi}\chi - \frac{1}{2}f_1\left(\overline{\chi^C}P_L\chi + \text{h.c.}\right)\eta^\star - \frac{1}{2}f_2\left(\overline{\chi^C}P_R\chi + \text{h.c.}\right)\eta^\star, \tag{33}$$

where f_1 and f_2 are the interaction strengths to left and right components of the vector-like fermion χ. When η gets a vev, the DM gets small Majorana mass $m_L = f_1 v_\eta$ and $m_R = f_2 v_\eta$. The presence of small Majorana mass terms for the DM split the Dirac state into two real Majorana states χ_1 and χ_2. The Lagrangian in terms of the new eigenstates is given as

$$\begin{aligned}\mathcal{L}_{DM} = {}& \frac{1}{2}\overline{\chi_1}i\gamma^\mu\partial_\mu\chi_1 - \frac{1}{2}M_1\overline{\chi_1}\chi_1 + \frac{1}{2}\overline{\chi_2}i\gamma^\mu\partial_\mu\chi_2 - \frac{1}{2}M_2\overline{\chi_2}\chi_2 + ig_{\mu\tau}\overline{\chi_2}\gamma^\mu\chi_1\,Z'_\mu \\ & + \frac{1}{2}g_{\mu\tau}\frac{m_-}{M_\chi}\left(\overline{\chi_2}\gamma^\mu\gamma^5\chi_2 - \overline{\chi_1}\gamma^\mu\gamma^5\chi_1\right)Z'_\mu + \mathcal{O}(\frac{m_-^2}{M_\chi^2}) \\ & + \frac{1}{2}\left(f_1\cos^2\theta - f_2\sin^2\theta\right)\overline{\chi_1}\chi_1\eta + \frac{1}{2}\left(f_2\cos^2\theta - f_1\sin^2\theta\right)\overline{\chi_2}\chi_2\eta\,,\end{aligned} \tag{34}$$

where $\sin\theta$ is the mixing angle, M_1 and M_2 are the two mass eigenvalues and are given by

$$M_1 = M_\chi - m_+,\ M_2 = M_\chi + m_+, \tag{35}$$

$$m_\pm = \frac{m_L \pm m_R}{2}. \tag{36}$$

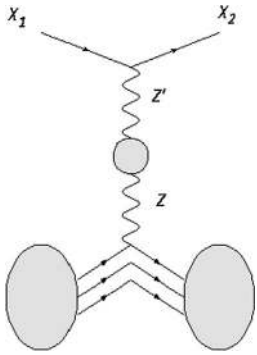

Fig. 8. Inelastic scattering of DM with the target nucleus through the Z–Z' mixing.

From the above expression the dominant gauge interaction is off-diagonal, and the diagonal interaction is suppressed as $\frac{m_-}{M_\chi} \ll 1$. The mass splitting between the two mass eigen-states is given by

$$\delta = M_2 - M_1 = 2m_+ = (f_1 + f_2)v_\eta\,. \tag{37}$$

The inelastic scattering with the target nucleus due to Z–Z' mixing is shown in Fig. 8. The occurrence of this process solely depends on the mass splitting between the two states. In fact, the minimum velocity of the DM needed to register a recoil inside the detector is given by [66–70]

$$v_{\min} = c\sqrt{\frac{1}{2m_n E_R}}\left(\frac{m_n E_R}{\mu_r} + \delta\right), \tag{38}$$

where E_R is the recoil energy of the nucleon. If the mass splitting is above a few hundred keV, then it will be difficult to excite χ_2. So the inelastic scattering will be forbidden.

8. Indirect detection of DM

We now look at the compatibility of the present framework with indirect detection signals of DM and in particular AMS-02 positron data. Recently, the AMS-02 experiment reported the results of high precision measurement of the cosmic ray positron fraction in the energy range of 0.5–500 GeV [50,51]. This result further confirmed the measurement of an excess in the positron fraction above 10 GeV as observed by PAMELA [47,48] and FERMI-LAT [49]. The usual explanation for this excess is through DM annihilation producing the required flux of positrons. However such an excess was not observed in the antiproton flux by PAMELA [71], thus suggesting a preference for leptonic annihilation channels. Recently AMS-02 also announced results from their measurement of the antiproton flux, which suggests a slight excess above 100 GeV [72]. But this was found to be within error of the modeling of secondary astrophysical production [73]. In this context we consider the $L_\mu - L_\tau$ symmetry where the DM dominantly annihilates to muons which then subsequently decay to produce electrons. This ensures a softer distribution of positrons thereby providing a better fit to the experimental data.

For theoretical explanation for AMS-02 positron excess through DM annihilations in the $L_\mu - L_\tau$ symmetric extension of SM we have to calculate propagation of cosmic rays in the galaxy. In order to do this calculation, the propagation of cosmic rays is treated as a diffusion process and one therefore solves the appropriate diffusion equation. Here we calculate the flux of the cosmic

ray electrons (primary and secondary) as well as secondary positrons at the position of the sun after propagating through the galaxy. The propagation equation for charged cosmic rays is given by [74]

$$\frac{\partial\psi(\vec{r},p)}{\partial t} = q + \vec{\nabla}\cdot\left(D_{xx}\vec{\nabla}\psi - \vec{V}_c\psi\right) + \frac{\partial}{\partial p}p^2 D_{pp}\frac{\partial}{\partial p}\frac{1}{p^2}\psi - \frac{\partial}{\partial p}\left[\dot{p}\psi - \frac{p}{3}\left(\vec{\nabla}\cdot\vec{V}_c\right)\psi\right] - \frac{1}{\tau_f}\psi - \frac{1}{\tau_r}\psi \tag{39}$$

where ψ is the cosmic ray density, $\dot{p}$ gives the energy loss of cosmic rays, $D_{xx(pp)}$ is the diffusion coefficient in spatial (momentum) coordinates while the last two terms represent the fragmentation and radioactive decay of cosmic ray nuclei. The diffusion coefficient is parameterized as $D_{xx} = D_{0xx}E^{-\gamma_e-\delta}$. The primary spectrum of cosmic ray electrons is modeled by

$$\psi = \frac{N}{2}\frac{L}{D_{0xx}}E^{-\gamma_e-\delta} \tag{40}$$

where N is a normalization constant and L is the half height of the cylindrical diffusion zone. The parameters for propagation of cosmic rays are D_0, δ, N, L, v_a (Alfven velocity), V_c and γ_e. We use the GALPROP package [75] to solve the diffusion equation in Eq. (39) using a diffusive re-acceleration model of diffusion. The cosmic ray primary and secondary electron flux as well as the secondary positron flux which constitute the astrophysical background are thus obtained. The positron flux from DM annihilations is calculated using `micrOMEGAs` [58] while the gauged $U(1)_{L_\mu - L_\tau}$ model is implemented in `micrOMEGAs` with the help of LanHEP [76]. The ratio of the DM positron signal thus obtained, to the total astrophysical background gives the positron fraction.

The key feature of this model is that the DM does not couple to quarks at tree level and hence we do not see any observable contribution to the antiproton flux. We therefore focus on the possible explanation of positron fraction. However, from Fig. 3, we noticed that the combine constraints from muon $g-2$ anomaly and neutrino trident production restricts the $M_{Z'} \lesssim 400$ MeV and $g_{\mu\tau} \lesssim 10^{-3}$. In this limited parameter space, the DM annihilation cross section $\langle\sigma|v|\rangle(\chi^\dagger\chi \to \mu^+\mu^-, \tau^+\tau^-) << \langle\sigma|v|\rangle_F \equiv 3\times 10^{-26}$ cm^3/s. Therefore, to explain the observed positron excess one needs an unnaturally large boost factor. As we describe below, the most favorable cross-section for DM annihilation to positrons that explains the AMS-02 positron excess occurs near the resonance, Z' mass of $2M_\chi$, with the DM–Z' coupling $\sim 10^{-1}$, which is now ruled out by the combine constraints from $g-2$ anomaly and neutrino trident production. Thus one finds that a reasonable explanation of the AMS-02 positron excess in the $L_\mu - L_\tau$ model under consideration is ruled out. However, if we choose any point below the dashed brown curve of Fig. 3, then these points are not ruled out by neutrino trident production though contribute partially to anomalous $g-2$ values. In this region of parameter space, the DM annihilation can explain the observed positron excess while being compatible with relic density and direct detection limits. We consider two benchmark points which satisfy the relic density constraint from PLANCK [5]. The parameters for the two chosen benchmark points are listed in Table 2. We find that for the best fit to AMS-02 data in the current scenario requires $M_\chi \gtrsim 500$ GeV. Also for satisfying the relic density constraint we need $M_{Z'} \sim 500$ GeV for $M_\chi \gtrsim 500$ GeV. (See Fig. 9.)

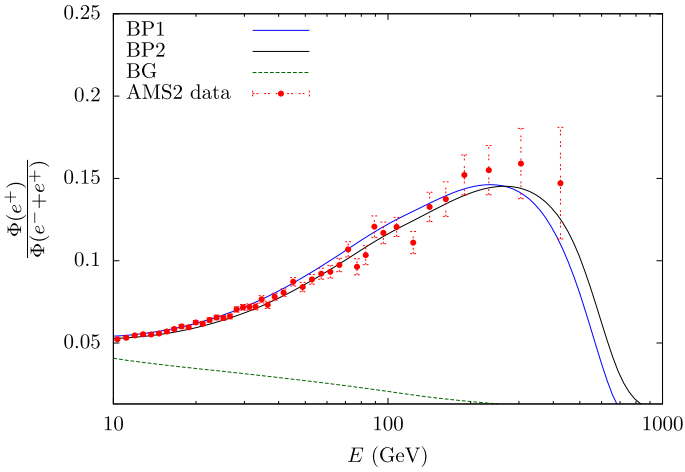

Fig. 9. Ratio of positron flux to the total $(e^- + e^+)$ flux against energy of the cosmic rays with AMS-02(2014) data [51] for benchmark points listed in Table 2. The blue curve is for the benchmark point BP1 while the black curve is for BP2. (For interpretation of the references to color in this figure, the reader is referred to the web version of this article.)

Table 2
Benchmark point which satisfies relic density and fits the AMS2 positron fraction data [51].

	M_χ (GeV)	$M_{Z'}$ (GeV)	$g_{\mu\tau}$	Ωh^2	Boost factor
BP1	710	838	0.35	0.116	720
BP2	800	782	0.4	0.113	800

9. Conclusion

We discussed a gauged $U(1)_{L_\mu - L_\tau}$ extension of the SM in light of the non-zero neutrino mass, DM and the observed muon $g-2$ anomaly which is a more than 3σ discrepancy between the experimental measurement and the SM prediction. In addition to that, three right handed neutrinos N_e, N_μ, N_τ and a Dirac fermion χ were introduced which are charged under $U(1)_{L_\mu - L_\tau}$ symmetry except N_e which is a complete singlet fermion. The $U(1)_{L_\mu - L_\tau}$ was allowed to break completely at a TeV scale by giving vev to a SM singlet scalar S which bears an unit $L_\mu - L_\tau$ charge. The vev of S gave masses not only to the additional gauge boson Z', but also to the right handed neutrinos: N_e, N_μ, N_τ. As a result, below electroweak symmetry breaking, the light neutrinos acquired masses through the type-I seesaw mechanism. Under the Z_2 symmetry, χ was chosen to be odd while rest of the particles were even. Thus χ became an excellent candidate of DM.

We obtained the relic abundance of DM via its annihilation to muon and tauon families of leptons through the exchange of Z' gauge boson. It is found that for Z' mass greater than 100 MeV and its coupling to leptons: $g_{\mu\tau} > 5 \times 10^{-3}$ correct relic abundance can be obtained. On the other hand, the muon $g-2$ anomaly requires smaller values of the gauge coupling $g_{\mu\tau}$ for Z' mass greater than 100 MeV (see Fig. 3). So the two problems could not be solved simultaneously. Therefore, we introduced an additional scalar η which is doubly charged under $U(1)_{L_\mu - L_\tau}$ but singlet under the SM gauge group. In presence of η, the DM dominantly annihilates to η fields.

As a result we found a large region of parameter space in which the constraints from muon $g-2$ anomaly and relic abundance of DM could be satisfied simultaneously. The hitherto null detection of DM at direct search experiments, such as LUX, is also discussed in Fig. 3. We found that the constraints from muon $g-2$ anomaly and LUX experiment are compatible in a large parameter space.

The combine constraints from muon $g-2$ anomaly and neutrino trident production restricts $M_{Z'} \lesssim 400$ MeV and $g_{\mu\tau} \lesssim 10^{-3}$. This restricted parameter space is compatible with muon $g-2$ anomaly, latest direct detection limits from LUX and relic abundance of DM in presence of η field. In this limited parameter space the annihilation cross-section of DM to muon and tauon pairs through the exchange of Z' is much smaller than the DM relic abundance cross-section. So one needs unnaturally large boost factor to explain the observed positron flux by PAMELA, Fermi-LAT and recently by AMS-02 in the cosmic ray shower. However, if we consider the parameter space in the plane of $g_{\mu\tau}$ versus $M_{Z'}$, which is not constrained by neutrino trident production, i.e., points below the brown dashed curve, then we can explain the observed positron excess by DM annihilation with suppressed antiproton flux, as in our model the DM annihilates only to lepton pairs. Note that these points in the plane of $g_{\mu\tau}$ versus $M_{Z'}$ contribute partially to the anomalous $g-2$ anomaly. Thus, while explaining the observed positron excess, we need to sacrifice the explanation for $g-2$ anomaly and vice versa.

Acknowledgements

The work of SR is supported by the University of Adelaide and the Australian Research Council through the ARC Center of Excellence in Particle Physics at the Terascale. Narendra Sahu is partially supported by the Department of Science and Technology, Govt. of India under the financial Grant SR/FTP/PS-209/2011. We thank Workshop on High Energy Physics Phenomenology (WHEPP)-XIV, held at IIT Kanpur during 4–13 December 2015, where a part of this work was done.

References

[1] J.P. Miller, E. de Rafael, B.L. Roberts, Rep. Prog. Phys. 70 (2007) 795, arXiv:hep-ph/0703049.
[2] S. Fukuda, et al., Super-Kamiokande Collaboration, Phys. Rev. Lett. 86 (2001) 5656, arXiv:hep-ex/0103033.
[3] G. Bertone, D. Hooper, J. Silk, Phys. Rep. 405 (2005) 279, arXiv:hep-ph/0404175;
G. Jungman, M. Kamionkowski, K. Griest, Phys. Rep. 267 (1996) 195, arXiv:hep-ph/9506380.
[4] G. Hinshaw, et al., WMAP Collaboration, Astrophys. J. Suppl. Ser. 208 (2013) 19, arXiv:1212.5226 [astro-ph.CO].
[5] P.A.R. Ade, et al., Planck Collaboration, Astron. Astrophys. 571 (2014) A16, arXiv:1303.5076 [astro-ph.CO].
[6] X.G. He, G.C. Joshi, H. Lew, R.R. Volkas, Phys. Rev. D 43 (1991) 22.
[7] X.g. He, arXiv:hep-ph/9409237.
[8] S. Baek, N.G. Deshpande, X.G. He, P. Ko, Phys. Rev. D 64 (2001) 055006, arXiv:hep-ph/0104141.
[9] W. Altmannshofer, M. Carena, A. Crivellin, arXiv:1604.08221 [hep-ph].
[10] W. Altmannshofer, S. Gori, M. Pospelov, I. Yavin, Phys. Rev. D 89 (2014) 095033, arXiv:1403.1269 [hep-ph].
[11] J. Heeck, Phys. Lett. B 758 (2016) 101, arXiv:1602.03810 [hep-ph].
[12] K. Fuyuto, W.S. Hou, M. Kohda, Phys. Rev. D 93 (5) (2016) 054021, arXiv:1512.09026 [hep-ph].
[13] A. Crivellin, G. D'Ambrosio, J. Heeck, Phys. Rev. D 91 (7) (2015) 075006, arXiv:1503.03477 [hep-ph].
[14] A. Crivellin, G. D'Ambrosio, J. Heeck, Phys. Rev. Lett. 114 (2015) 151801, arXiv:1501.00993 [hep-ph].
[15] J. Heeck, M. Holthausen, W. Rodejohann, Y. Shimizu, Nucl. Phys. B 896 (2015) 281, arXiv:1412.3671 [hep-ph].
[16] E. Ma, D.P. Roy, arXiv:hep-ph/0111385.
[17] K. Harigaya, T. Igari, M.M. Nojiri, M. Takeuchi, K. Tobe, J. High Energy Phys. 1403 (2014) 105, arXiv:1311.0870 [hep-ph].
[18] F. Elahi, A. Martin, Phys. Rev. D 93 (1) (2016) 015022, arXiv:1511.04107 [hep-ph].

[19] E. Ma, D.P. Roy, S. Roy, Phys. Lett. B 525 (2002) 101, arXiv:hep-ph/0110146.
[20] J. Heeck, W. Rodejohann, Phys. Rev. D 84 (2011) 075007, arXiv:1107.5238 [hep-ph].
[21] J. Heeck, W. Rodejohann, AIP Conf. Proc. 1382 (2011) 144, arXiv:1012.2298 [hep-ph].
[22] J. Heeck, W. Rodejohann, J. Phys. G 38 (2011) 085005, arXiv:1007.2655 [hep-ph].
[23] T. Ota, W. Rodejohann, Phys. Lett. B 639 (2006) 322, arXiv:hep-ph/0605231.
[24] W. Rodejohann, M.A. Schmidt, Phys. At. Nucl. 69 (2006) 1833, arXiv:hep-ph/0507300.
[25] Z.z. Xing, Z.h. Zhao, arXiv:1512.04207 [hep-ph].
[26] D.C. Rivera-Agudelo, A. Pérez-Lorenzana, arXiv:1603.02336 [hep-ph].
[27] S. Choubey, W. Rodejohann, Eur. Phys. J. C 40 (2005) 259, arXiv:hep-ph/0411190.
[28] X.G. He, G.C. Joshi, H. Lew, R.R. Volkas, Phys. Rev. D 44 (1991) 2118.
[29] T. Araki, F. Kaneko, T. Ota, J. Sato, T. Shimomura, Phys. Rev. D 93 (1) (2016) 013014, arXiv:1508.07471 [hep-ph].
[30] E. Salvioni, A. Strumia, G. Villadoro, F. Zwirner, J. High Energy Phys. 1003 (2010) 010, arXiv:0911.1450 [hep-ph].
[31] B. Adhikary, Phys. Rev. D 74 (2006) 033002, arXiv:hep-ph/0604009.
[32] N.F. Bell, R.R. Volkas, Phys. Rev. D 63 (2001) 013006, arXiv:hep-ph/0008177.
[33] K. Fuki, M. Yasue, Nucl. Phys. B 783 (2007) 31, arXiv:hep-ph/0608042.
[34] S. Baek, H. Okada, K. Yagyu, J. High Energy Phys. 1504 (2015) 049, arXiv:1501.01530 [hep-ph].
[35] B. Shuve, I. Yavin, Phys. Rev. D 89 (11) (2014) 113004, arXiv:1403.2727 [hep-ph].
[36] P.f. Yin, J. Liu, S.h. Zhu, Phys. Lett. B 679 (2009) 362, arXiv:0904.4644 [hep-ph].
[37] X.J. Bi, X.G. He, Q. Yuan, Phys. Lett. B 678 (2009) 168, arXiv:0903.0122 [hep-ph].
[38] J.C. Park, S.C. Park, J. Kim, Phys. Lett. B 752 (2016) 59, arXiv:1505.04620 [hep-ph].
[39] S. Baek, Phys. Lett. B 756 (2016) 1, arXiv:1510.02168 [hep-ph].
[40] S. Baek, P. Ko, J. Cosmol. Astropart. Phys. 0910 (2009) 011, arXiv:0811.1646 [hep-ph].
[41] M. Carena, A. Daleo, B.A. Dobrescu, T.M.P. Tait, Phys. Rev. D 70 (2004) 093009, arXiv:hep-ph/0408098.
[42] E. Aprile, et al., XENON100 Collaboration, Phys. Rev. Lett. 109 (2012) 181301, arXiv:1207.5988 [astro-ph.CO].
[43] D.S. Akerib, et al., LUX Collaboration, Phys. Rev. Lett. 112 (2014) 091303, arXiv:1310.8214 [astro-ph.CO].
[44] W. Altmannshofer, S. Gori, M. Pospelov, I. Yavin, Phys. Rev. Lett. 113 (2014) 091801, arXiv:1406.2332 [hep-ph].
[45] D. Geiregat, et al., CHARM-II Collaboration, Phys. Lett. B 245 (1990) 271.
[46] S.R. Mishra, et al., CCFR Collaboration, Phys. Rev. Lett. 66 (1991) 3117.
[47] O. Adriani, et al., PAMELA Collaboration, Nature 458 (2009) 607, arXiv:0810.4995 [astro-ph].
[48] O. Adriani, et al., Astropart. Phys. 34 (2010) 1, arXiv:1001.3522 [astro-ph.HE].
[49] M. Ackermann, et al., Fermi-LAT Collaboration, Phys. Rev. Lett. 108 (2012) 011103, arXiv:1109.0521 [astro-ph.HE].
[50] M. Aguilar, et al., AMS Collaboration, Phys. Rev. Lett. 110 (2013) 141102.
[51] L. Accardo, et al., AMS Collaboration, Phys. Rev. Lett. 113 (2014) 121101.
[52] K. Jedamzik, M. Pospelov, New J. Phys. 11 (2009) 105028, arXiv:0906.2087 [hep-ph].
[53] M. Kawasaki, K. Kohri, T. Moroi, Phys. Rev. D 71 (2005) 083502, arXiv:astro-ph/0408426.
[54] C. Arina, F.X. Josse-Michaux, N. Sahu, Phys. Rev. D 82 (2010) 015005, arXiv:1004.3953 [hep-ph].
[55] M. Kaplinghat, S. Tulin, H.B. Yu, Phys. Rev. D 89 (3) (2014) 035009, arXiv:1310.7945 [hep-ph].
[56] K.A. Olive, et al., Particle Data Group, Chin. Phys. C 38 (2014) 090001.
[57] G.W. Bennett, et al., Muon g-2 Collaboration, Phys. Rev. D 73 (2006) 072003, arXiv:hep-ex/0602035.
[58] G. Bélanger, F. Boudjema, A. Pukhov, A. Semenov, Comput. Phys. Commun. 192 (2015) 322, arXiv:1407.6129 [hep-ph].
[59] M.W. Goodman, E. Witten, Phys. Rev. D 31 (1985) 3059.
[60] R. Essig, Phys. Rev. D 78 (2008) 015004, arXiv:0710.1668 [hep-ph].
[61] R. Koch, Z. Phys. C 15 (1982) 161;
J. Gasser, H. Leutwyler, M.E. Sainio, Phys. Lett. B 253 (1991) 260;
M.M. Pavan, R.A. Arndt, I.I. Strakovski, R.L. Workman, PiN Newslett. 16 (2002) 110;
A. Bottino, F. Donato, N. Fornengo, S. Scopel, Phys. Rev. D 78 (2008) 083520, arXiv:0806.4099.
[62] A. Hook, E. Izaguirre, J.G. Wacker, Adv. High Energy Phys. 2011 (2011) 859762, arXiv:1006.0973 [hep-ph].
[63] K.S. Babu, C.F. Kolda, J. March-Russell, Phys. Rev. D 57 (1998) 6788, arXiv:hep-ph/9710441.
[64] M. Hoferichter, J. Ruiz de Elvira, B. Kubis, U.G. Meißner, Phys. Rev. Lett. 115 (2015) 092301, arXiv:1506.04142 [hep-ph].
[65] A. Crivellin, M. Hoferichter, M. Procura, Phys. Rev. D 89 (2014) 054021, arXiv:1312.4951 [hep-ph].
[66] D. Tucker-Smith, N. Weiner, Phys. Rev. D 64 (2001) 043502, arXiv:hep-ph/0101138.
[67] Y. Cui, D.E. Morrissey, D. Poland, L. Randall, J. High Energy Phys. 0905 (2009) 076, arXiv:0901.0557 [hep-ph].
[68] C. Arina, N. Sahu, Nucl. Phys. B 854 (2012) 666, arXiv:1108.3967 [hep-ph].

[69] C. Arina, J.O. Gong, N. Sahu, Nucl. Phys. B 865 (2012) 430, arXiv:1206.0009 [hep-ph].
[70] C. Arina, R.N. Mohapatra, N. Sahu, Phys. Lett. B 720 (2013) 130, arXiv:1211.0435 [hep-ph].
[71] O. Adriani, et al., PAMELA Collaboration, Phys. Rev. Lett. 105 (2010) 121101, arXiv:1007.0821 [astro-ph.HE].
[72] AMS-02 Collaboration, Talks at the 'AMS Days at CERN', April 2015, pp. 15–17.
[73] G. Giesen, M. Boudaud, Y. Génolini, V. Poulin, M. Cirelli, P. Salati, P.D. Serpico, J. Cosmol. Astropart. Phys. 1509 (09) (2015) 023, arXiv:1504.04276 [astro-ph.HE].
[74] A.W. Strong, I.V. Moskalenko, V.S. Ptuskin, Annu. Rev. Nucl. Part. Sci. 57 (2007) 285, arXiv:astro-ph/0701517.
[75] I.V. Moskalenko, A.W. Strong, Astrophys. J. 493 (1998) 694, arXiv:astro-ph/9710124;
A.E. Vladimirov, et al., Comput. Phys. Commun. 182 (2011) 1156, arXiv:1008.3642 [astro-ph.HE].
[76] A.V. Semenov, arXiv:hep-ph/9608488.